Batteries & Supercaps

Research Article
doi.org/10.1002/batt.202400009

Chemistry Europe
European Chemical Societies Publishing

www.batteries-supercaps.org

Application of Na_2CO_3 as a Sacrificial Electrode Additive in Na-ion Batteries to Compensate for the Sodium Deficiency in $Na_{2/3}[Fe_{1/2}Mn_{1/2}]O_2$

Masayoshi Matsuzaki,[a] Ryoichi Tatara,[a] Kei Kubota+,[a] Kazutoshi Kuroki,[a] Tomooki Hosaka,[a] Kazuteru Umetsu,[b] Nobuhiro Okada,[c] and Shinichi Komaba*[a]

Owing to their high discharge capacities, P2-type transition metal layered oxides have attracted attention for use as positive electrode materials in Na-ion batteries. However, owing to the Na-deficient compositions of these oxides, additional Na^+ must be supplied using a Na-metal negative electrode to attain a high capacity in a half-cell configuration. In this study, solid Na_2CO_3 powder was introduced into the P2–$Na_{2/3}Fe_{1/2}Mn_{1/2}O_2$ composite positive electrode as a sacrificial salt to compensate for the Na deficiency. Na^+ was supplied through the electrochemical oxidative decomposition of Na_2CO_3 during the initial charging process; the decomposition mechanism responsible for this process was investigated in detail. Online electrochemical mass spectrometry confirmed that Na_2CO_3 was oxidatively decomposed in combination with the decomposition of the ethylene carbonate electrolyte. This reaction produced CO_2, wherein the carbon source was derived from both Na_2CO_3 and the electrolyte. Consequently, Na^+ supplementation improved the reversible capacity of the Na-ion full cell. This study offers practical insights and a mechanistic understanding of the pre-doping technique for Na-free negative electrodes. This approach also compensates for the irreversible reductive capacity in a process that can be easily applied to practical sodium- and lithium-ion batteries and capacitors.

1. Introduction

Sodium-ion batteries have attracted significant attention in recent years because of the greater abundance, widespread distribution, and lower cost of Na resources compared to those of lithium.[1] Indeed, since the Na_xCoO_2 electrode was first studied by Delmas et al. in the 1980s, various layered oxide materials for use as positive electrodes in sodium-ion batteries have been reported.[2] In addition, in 2009, our group demonstrated the good reversibility and phase evolution of O3-type $NaNi_{1/2}Mn_{1/2}O_2$ and $NaCrO_2$ electrodes in nonaqueous Na cells.[3] Subsequently, we reported the excellent rate performance of O3-type $NaFe_{1/2}Co_{1/2}O_2$,[4] and the high capacity of P2-type $Na_{2/3}Fe_{1/2}Mn_{1/2}O_2$.[5] In these systems, O3 and P2 represent the structures of the layered oxides; O signifies that Na occupies octahedral sites, whereas P indicates that prismatic sites are occupied. The number following the letter corresponds to the number of transition-metal slabs in the unit cell.[2a] Typically, positive electrode materials with O3-type structures possess an initial Na composition close to $x = 1$ in Na_xMeO_2 (Me = a metal, normally a transition metal). However, the initial composition of Na in the P2-type structure was found to be $x \approx 0.7$, which is less than that of the O3-type material.[1a,2c] By compensating for the Na-deficient composition in the P2-type structure of the positive electrode, it is possible to achieve a higher discharge capacity (i.e., Na insertion; cf., the charge or Na extraction capacity) in a half-cell with a Na metal negative electrode. In contrast, full cells utilizing Na-free hard carbon[6] as the negative electrode exhibit lower discharge capacities owing to insufficient Na supplementation when the anode/cathode (A/C) ratio is fixed by balancing the charge capacities of both the anode and cathode. Furthermore, the hard-carbon negative electrode forms a solid electrolyte interphase (SEI) on the electrode surface via electrolyte decomposition during the first charging cycle, resulting in an irreversible capacity contribution from the negative electrode.[6c,7] This irreversible capacity during the first charge does not contribute to Na^+ storage in the negative electrode; thus, the simultaneous irreversible Na extraction from the positive electrode resulted in a further decrease in the utilization of Na^+ at the positive electrode.[6b,8] It is therefore desirable to compensate for the Na deficiency in P2-type layered oxide positive electrodes and to address the irreversible capacity of negative electrodes by the supplementation of Na^+

[a] M. Matsuzaki, R. Tatara, K. Kubota,+ K. Kuroki, T. Hosaka, S. Komaba
Department of Applied Chemistry, Tokyo University of Science, 1–3 Kagurazaka, Shinjuku, Tokyo 162-8601, Japan
E-mail: komaba@rs.tus.ac.jp

[b] K. Umetsu
R&D Center, Asahi Kasei Europe GmbH, Fringsstraße 17, 40221 Düsseldorf, Germany

[c] N. Okada
Energy Solution Laboratory, Corporate Research & Development, Asahi Kasei Corporation, 2-1 Samejima, Fuji, Shizuoka 416-8501, Japan

[+] present address: Center for Green Research on Energy and Environmental Materials (GREEN), National Institute for Materials Science (NIMS), 1-1 Namiki, Tsukuba, Ibaraki, 305-0044, Japan

Supporting information for this article is available on the WWW under https://doi.org/10.1002/batt.202400009

Research Article
doi.org/10.1002/batt.202400009
Chemistry Europe
European Chemical Societies Publishing

to ultimately increase the available capacity of the Na-ion full cell.

To address the above issues, Na^+ ions can be electrochemically or chemically inserted into the positive or negative electrodes by pre-doping.[9] Although pre-doping techniques are widely used in the preparation of Li-ion capacitors, they require either a direct chemical reaction between the electrode and the sacrificial Li metal,[10] or the pre-cycling of the negative electrode in a half-cell configuration with a Li metal counter electrode,[11] followed by reassembly to prepare a full cell.[12] Pre-doping with Na^+ (presodiation) has also been reported to compensate for Na^+ loss and improve the initial Coulombic efficiencies of sodium-ion battery systems.[13] However, such modifications introduce challenges in terms of the simplicity, safety, and costs of hard-carbon//P2–$Na_{2/3}Fe_{1/2}Mn_{1/2}O_2$ cells. As a cheaper alternative, sacrificial salts have recently been introduced into positive electrodes to supplement Na^+, including NaN_3,[14] Na_3P,[15] Na_2S,[16] $Na_2C_4O_4$,[17] $Na_2C_6O_6$,[18] $Na_2C_2O_4$,[19] $NaNO_2$,[20] and Na_2CO_3.[13,21] Sacrificial salts also hold potential benefits for anode-free battery systems, which suffer from challenges related to plating/stripping reversibility on the metal anode.[22] By mitigating the consumption of sodium sources, sacrificial salts could help improve the overall performance and durability of anode-free battery systems. A suitable sacrificial salt is a compound that electrochemically oxidizes and decomposes to release Na^+ into the electrolyte during the initial charge process. However, NaN_3 and Na_2S are explosive and/or toxic, and although salts such as $Na_2C_4O_4$, $Na_2C_6O_6$, and $Na_2C_2O_4$ are less hazardous, the calculated specific capacities obtained from their anodic decomposition tend to be $<400\ mAh\,g^{-1}$, leading to undesired weight gain in the full cell. In contrast, Na_2CO_3 is abundant, inexpensive, safe, and easy to handle. Assuming that its decomposition follows the reaction $Na_2CO_3 \rightarrow 2Na^+ + 2e^- + CO_2 + 1/2O_2$,[23] the calculated decomposition capacity is relatively high at $506\ mAh\,g^{-1}$, indicating the suitability of Na_2CO_3 as a particularly promising sacrificial salt. Although Sathiya et al. have reported that Na_2CO_3 yields Na^+ via anodic decomposition during the initial charging cycle,[21] the decomposition mechanism is not yet fully understood. In their study, the unreacted Na_2CO_3 remaining after the solid-state synthesis of the P2-type positive electrode material was found to remain on the surface of the P2-type product, it was deduced that this unreacted Na_2CO_3 consequently acted as a sacrificial salt. However, the optimal amount of Na_2CO_3 for use in the full-cell design was not determined. Another recent study involved the addition of Na_2CO_3 as a sacrificial salt to the activated carbon positive electrode of a Na-ion capacitor to compensate for the lack of Na^+.[24] However, the comprehensive decomposition mechanism of Na_2CO_3 remained unclear.

Thus, as illustrated in Figure 1, we herein report the addition of powdered Na_2CO_3 as a sacrificial salt to a Na-deficient layered oxide positive electrode, namely the P2-type $Na_{2/3}Fe_{1/2}Mn_{1/2}O_2$ (P2–FeMn).[5] The aims of this study are to increase the capacity of the full cell in conjunction with a hard-carbon negative electrode and to investigate the decomposition mechanism of Na_2CO_3.

2. Results and Discussion

Initially, a suitable pre-treatment method for the commercially available Na_2CO_3 powder was developed prior to its addition to the positive electrode. This was necessary due to the large particle size and relatively high degree of water contamination in the commercial Na_2CO_3, which are expected to be detrimental to the sacrificial reaction. More specifically, such character-

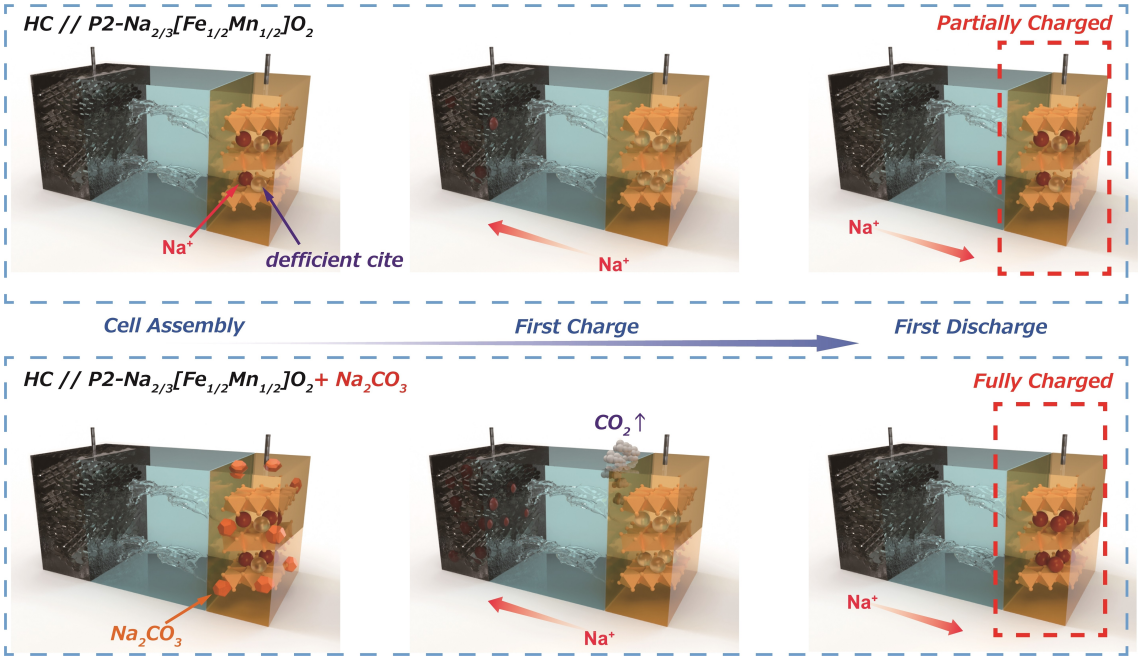

Figure 1. Schematic illustrations of the HC//P2–$Na_{2/3}Fe_{1/2}Mn_{1/2}O_2$ full cell with (bottom) and without (top) addition of the Na_2CO_3 sacrificial salt.

Research Article
doi.org/10.1002/batt.202400009
Chemistry Europe
European Chemical Societies Publishing

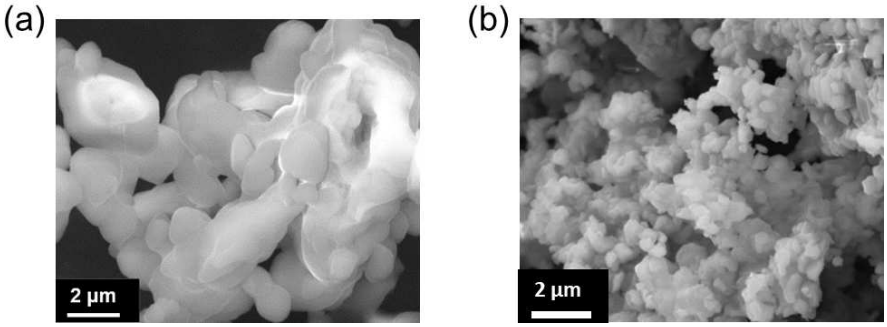

Figure 2. SEM images of the Na_2CO_3 specimens: (a) As purchased, and (b) after ball-milling and drying.

istics could lead to an increase in the interfacial resistance of the positive electrode, thereby highlighting the necessity to carry out a pre-treatment step aimed at reducing the particle size and drying the powder. Thus, Na_2CO_3 was initially dry-mixed and crushed via ball milling using ZrO_2 balls prior to drying at 200 °C under vacuum. As shown in Figure 2, the crushing and drying process reduced the particle size from >1.0 µm to 0.1–0.5 µm. Unless otherwise noted, the pretreated (ball-milled and dried) Na_2CO_3 was used as the sacrificial additive in subsequent experiments. In addition, although the solubility of Na_2CO_3 in NMP is relatively high (20.8 g L^{-1}),[25] the amount of NMP in the slurry was limited (Na_2CO_3 concentration in the slurry $\approx$40 g L^{-1}), and so it was estimated that the complete dissolution of the Na_2CO_3 was not achieved. Furthermore, the solubility of Na_2CO_3 in PC is known to be 6.6 mg L^{-1},[26] indicating that an electrolyte volume of <100 µL in the coin cell can dissolve <0.66 µg of Na_2CO_3 from the composite electrode; this would have a negligible effect on the battery performance.

Cyclic voltammetry (CV) was performed on the Co_3O_4 composite electrode in the presence (5 and 10 wt.%) and absence of Na_2CO_3 to investigate the decomposition behavior of this additive (Figure 3). Although it was expected that carbonate decomposition would be catalyzed by the P2-type $Na_{2/3}Fe_{1/2}Mn_{1/2}O_2$ surface, the cyclic voltammogram obtained for the electrode in the presence of Na_2CO_3 also exhibited redox peaks derived from the redox activity of the active material.[5,27] Consequently, it was difficult to distinguish the oxidation currents originating from the decomposition of Na_2CO_3 and from the extraction of Na from P2–$Na_{2/3}Fe_{1/2}Mn_{1/2}O_2$. Considering a previous report into the electrochemical decomposition of Li_2CO_3 using Co_3O_4 as an efficient electrocatalyst,[28] this electrocatalysis was employed herein for the decomposition of Na_2CO_3. As shown in the CV curve presented in Figure 3, in the absence of Na_2CO_3, the Co_3O_4 electrode exhibits an oxidation peak at ~4.5 V at a relatively small current, implying that the electrolyte can decompose and/or undergo anion insertion into the AB at high potentials. In contrast, in the presence of Na_2CO_3, the Co_3O_4 electrode exhibits an increase in its oxidation current beyond ~3.5 V, and demonstrates a sharp increases after ~4.0 V. Importantly, it was observed that the oxidation current increases in direct proportion to the amount of Na_2CO_3 added (i.e., 5 or 10 wt.%). The corresponding cathodic current was not

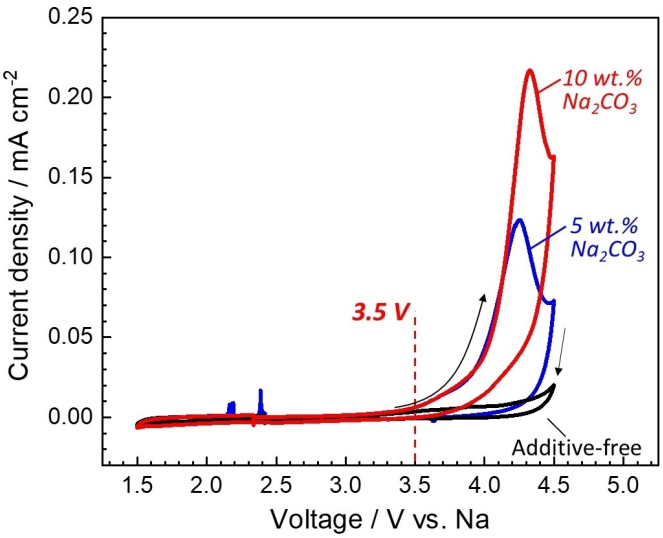

Figure 3. Cyclic voltammograms of the Co_3O_4 composite electrode in the presence and absence of Na_2CO_3 (5 and 10 wt.%). Measurements were carried out at 0.3 mV s^{-1} and 25 °C. The electrolyte consisted of a 1.0 mol dm^{-3} $NaPF_6$ solution in EC/PC, and Na metal was used as the counter electrode.

observed in either electrode even when scanning down to 1.5 V, indicating that the observed anodic reaction was irreversible. Elevated oxidation currents may therefore be associated with the decomposition of Na_2CO_3, which is initiated at >3.5 V and accelerates at >4.0 V. The anodic current caused by the decomposition of Na_2CO_3 exhibited a maximum at ~4.3 V; therefore, this was set as the upper voltage limit for subsequent tests.

Figure 4 shows the charge-discharge curves obtained for the Co_3O_4 electrodes both in the presence and absence of Na_2CO_3 (10 wt.%) in the Na metal half cells. While the charge capacity was almost zero for the electrode without any added Na_2CO_3 (Figure 4a), the electrode to which 10 wt.% Na_2CO_3 was added exhibited an irreversible capacity of 62 mAh $g_{(Co3O4)}^{-1}$ in the initial charging process (Figure 4b). This increase in the charge capacity was not observed during the subsequent cycles, indicating that the majority of Na_2CO_3 was sacrificed (i.e., oxidized and decomposed) in the first cycle. Figure 4c also reveals that the charge capacity obtained by holding the potential at 4.3 V for 3 h during CC–CV charging is increased to

Research Article
doi.org/10.1002/batt.202400009
Chemistry Europe
European Chemical Societies Publishing

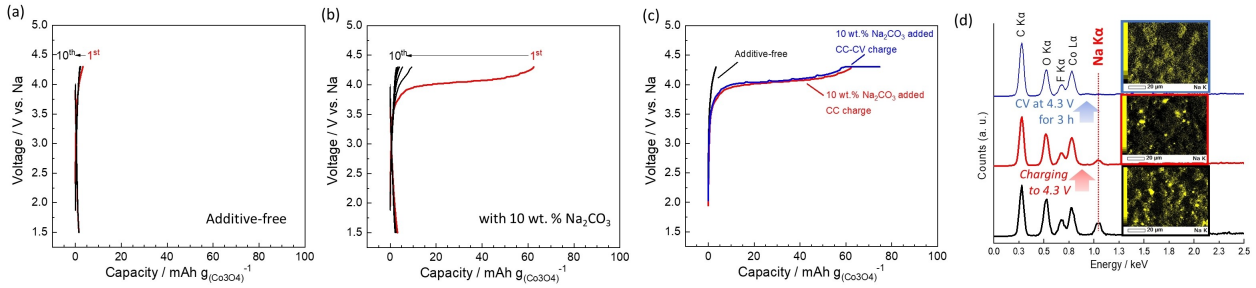

Figure 4. Charge-discharge curves of the Co_3O_4 composite electrode (a) in the absence of Na_2CO_3, and (b) in the presence of 10 wt.% Na_2CO_3 at 0.02 mA cm^{-2} and 25 °C. (c) Comparison of the initial charge capacities of the different systems. (d) EDS profiles and Na-EDS mapping images for the Na_2CO_3-added Co_3O_4 electrodes. The electrolyte consisted of a 1.0 mol dm^{-3} $NaPF_6$ solution in EC/PC, and Na metal was used as the counter electrode. CC denotes a constant current charge, while CC-CV denotes a constant current followed by a constant voltage charge.

74 mAh $g_{(Co3O4)}^{-1}$, which is in agreement with the calculated capacity of 72 mAh $g_{(Co3O4)}^{-1}$ (506 mAh $g_{(Na2CO3)}^{-1}$ ×1/7 = 72 mAh $g_{(Co3O4)}^{-1}$) obtained by the decomposition of 10 wt.% Na_2CO_3 (Co_3O_4:Na_2CO_3:AB:PVdF = 70:10:10:10). This indicates that constant-voltage charging ensures the decomposition of Na_2CO_3, which can be observed from the reduced Na Kα peak intensity in the SEM-EDS results for Na (see Figure 4d). In addition, the charge-discharge curves obtained at various current densities are presented in **Figure S1**, wherein it can be seen that the polarization increases and the charge capacity derived from the decomposition of Na_2CO_3 decreases with an increasing current density. This can be attributed to the insulating nature of Na_2CO_3 and the kinetic restraints surrounding electrochemical decomposition. With these results in mind, the initial charging reaction was conducted at a reasonably low current density of 0.02 mA cm^{-2}.

Following confirmation that Na_2CO_3 successfully decomposed on the Co_3O_4 electrode, Na_2CO_3 was applied as a sacrificial electrode additive for the P2-type $Na_{2/3}Fe_{1/2}Mn_{1/2}O_2$ composite positive electrode in a Na half-cell. **Figure S2** shows the charge-discharge curves of the P2-type $Na_{2/3}Fe_{1/2}Mn_{1/2}O_2$ electrodes containing 0, 5, and 10 wt.% Na_2CO_3, wherein it can be seen that the initial charge capacities were 164, 178, and 195 mAh (g^{-1}-$Na_{2/3}Fe_{1/2}Mn_{1/2}O_2$), respectively. This observation indicates that the addition of greater quantities of Na_2CO_3 increased the charge capacity associated with the Na_2CO_3 electro-oxidative decomposition. Although the discharge capacity decreased slightly with an increasing Na_2CO_3 content (likely due to the increased electrode resistance caused by an increase in the amount of insulating Na_2CO_3), the electrode containing 10 wt.% added Na_2CO_3 exhibited a relatively high discharge capacity of 185 mAh g^{-1}. In addition, **Figure S3** shows the effect of Na_2CO_3 pretreatment (i.e., ball milling and drying) on the battery performance. Although the addition of the as-purchased Na_2CO_3 greatly increased the overpotential, the ball milling and drying processes clearly reduced the degree of polarization, with the drying process being more effective in suppressing electrode polarization. To further promote the decomposition of Na_2CO_3 in the 10 wt.% system, the positive electrode was fully charged (initial charge) over a period of 3 h at a constant voltage of 4.3 V. As presented in Figure 5, the addition of 10 wt.% Na_2CO_3 led to a 64 mAh g^{-1} increase in the charge capacity (cf., in the absence of Na_2CO_3). Moreover, considering the mass of P2-type $Na_{2/3}Fe_{1/2}Mn_{1/2}O_2$ electrode, the calculated capacity based on the decomposition of 10 wt.% Na_2CO_3 was determined to be 72 mAh g^{-1}. Assuming that the observed increase in the charge capacity can be fully attributed to the decomposition of Na_2CO_3, it was inferred that 88% of the Na_2CO_3 was anodically decomposed in the composite, indicating an increase in the extent of Na_2CO_3 decomposition due to constant-voltage charging at a high potential.

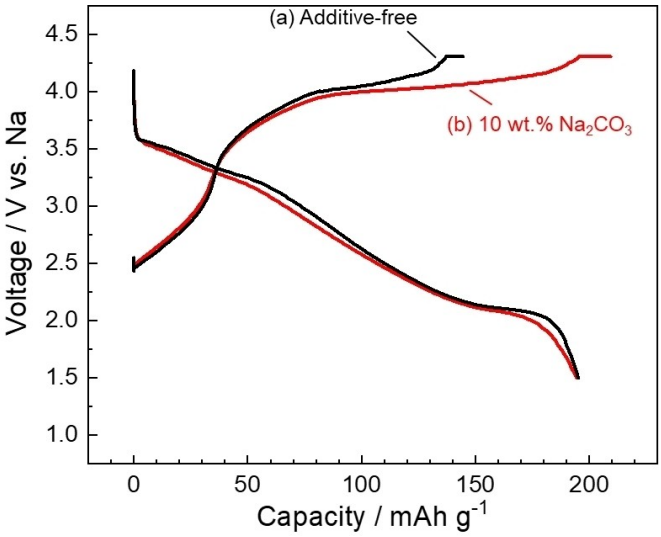

Figure 5. Charge-discharge curves for the P2–$Na_{2/3}Fe_{1/2}Mn_{1/2}O_2$//Na half cells upon the application of a constant voltage charge (4.3 V initial charge): (a) The additive-free cell, and (b) the cell containing 10 wt.% Na_2CO_3. All curves were measured at 0.02 mA cm^{-2} and 25 °C.

Based on the above observations, charge-discharge tests were performed for the full cells fabricated from the P2–$Na_{2/3}Fe_{1/2}Mn_{1/2}O_2$ positive electrode and the hard carbon negative electrode, as shown in Figure 6. It was confirmed that 3 h of constant-voltage charging (initial full charge) of the hard carbon electrode in the Na half-cell yielded an initial Coulombic efficiency of 83.2%, followed by a capacity retention of 95.8% after 50 cycles (**Figure S4**), thereby indicating its relevance to the full cell experiments. As shown in Figures 6a–6c, the full cell with 10 wt.% added Na_2CO_3 exhibits increased initial charge and discharge capacities relative to the full cell without Na_2CO_3.

Research Article
doi.org/10.1002/batt.202400009
Chemistry Europe
European Chemical Societies Publishing

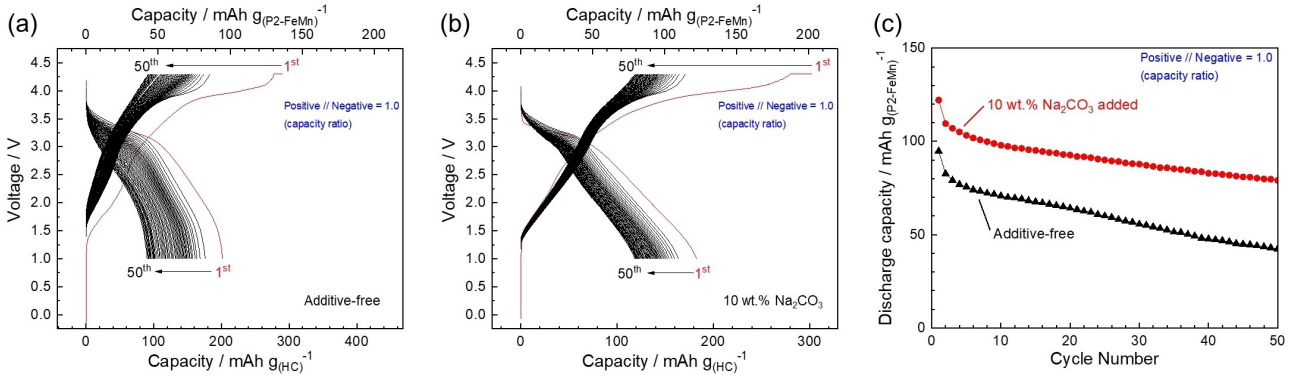

Figure 6. Charge-discharge curves of the HC//P2–$Na_{2/3}Fe_{1/2}Mn_{1/2}O_2$ full cells: (a) Additive-free, and (b) with the addition of 10 wt.% Na_2CO_3. These curves were measured at 25 °C. (c) Capacity retentions of the two systems. The upper horizontal axes in the charge-discharge curves indicate the capacity based on the mass of the positive electrode, while the lower horizontal axes provides the capacity based on the negative electrode. A constant voltage charge (3 h) was performed only for the initial charging process to completely decompose the sacrificial Na_2CO_3.

The addition of Na_2CO_3 was therefore beneficial to the operation of the positive electrode, and this could be attributed to Na^+ supplementation following electrochemical oxidative decomposition of the additive during the initial charging process. In addition, the P2–$Na_{2/3}Fe_{1/2}Mn_{1/2}O_2$ electrode with added Na_2CO_3 continued to demonstrate a high discharge capacity even after a number of cycles; the capacity retention after 50 cycles improved from 44.7 to 64.7% in the presence of Na_2CO_3. However, it should be noted that the half-cell exhibited a slightly lower capacity retention due to the slight polarization increase induced by the addition of Na_2CO_3 (**Figure S5**). Full-cell degradation was therefore believed to be caused in part by the discrepancy between the states-of-charge (SOCs) of the positive and negative electrodes during cycling, as previously reported for Li-ion batteries.[29] As mentioned above, the positive electrode containing no added Na_2CO_3 failed to undergo sufficient discharge owing to the inadequate supplementation of Na^+ from the negative electrode. In contrast, the full cell based on the Na_2CO_3-added positive electrode was fully discharged, resulting in a sufficiently low SOC. As the utilization rate of the positive electrode increased, the discrepancy between the SOCs of the positive and negative electrodes after cycling diminished, confirming that the addition of Na_2CO_3 to the positive electrode improved both the discharge capacity and the capacity retention of the full cell.

OEMS measurements were also performed to determine the decomposition of any gaseous products generated at the Na_2CO_3-containing P2-$Na_{2/3}Fe_{1/2}Mn_{1/2}O_2$ electrode. Figures 7 ($Na_2{}^{13}CO_3$ added) and **Figure S6** ($Na_2{}^{12}CO_3$ added) present the charge-discharge curves of the full cells used for these measurement along with the resulting MS intensities. Thus, O_2 ($m/z=32$), $^{12}CO_2$ ($m/z=44$), and $^{13}CO_2$ ($m/z=45$) were monitored by OEMS over two charge-discharge cycles. As shown in **Figure S6** ($Na_2{}^{12}CO_3$ added), the MS intensity at $m/z=44$ indicated that the content $^{12}CO_2$ increased beyond 3.4 V during the initial charge, and then decreased during the corresponding discharge. A negligible intensity was obtained in the second cycle for the $^{12}CO_2$ peak, indicating that the $^{12}CO_2$ gas ($m/z=44$) that evolved in the first cycle originated from the decomposition of

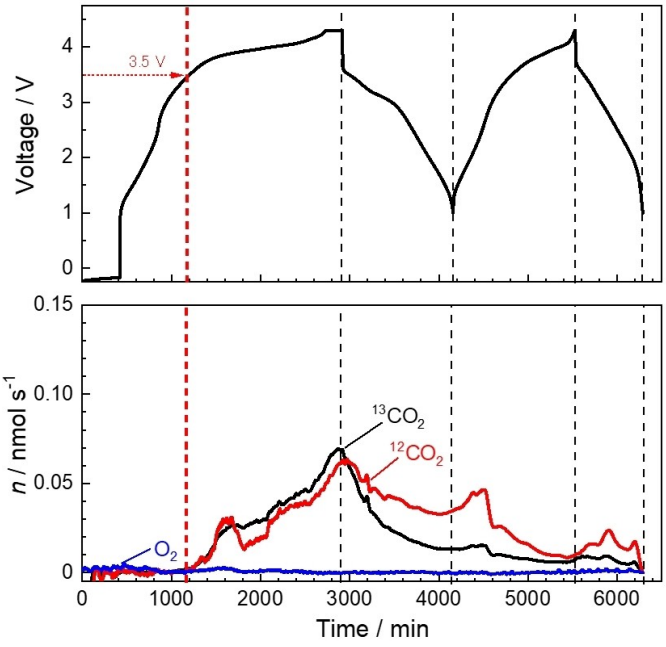

Figure 7. Charge-discharge curves and gas evolution rates (derived from the MS intensities) for O_2 ($m/z=32$), $^{12}CO_2$ ($m/z=44$), and $^{13}CO_2$ ($m/z=45$) during the OEMS measurements carried out on the HC//P2–$Na_{2/3}Fe_{1/2}Mn_{1/2}O_2$ full cell with 10 wt.% added $Na_2{}^{13}CO_3$. The background signal for the MS intensity was subtracted by fitting the baseline.

Na_2CO_3. In contrast, the intensity of the O_2 signal ($m/z=32$) was negligible, as observed in **Figure S6**. Although the generation of $^{12}CO_2$ was confirmed, it was not possible to determine whether this CO_2 originated from the decomposition of Na_2CO_3 or from other components of the battery cell. Therefore, the same OEMS test was conducted using ^{13}C-labeled Na_2CO_3 as the sacrificial salt (Figure 7). As a result, the observed evolution of $^{13}CO_2$ gas beyond 3.5 V during the initial charge indicated that the sacrificial salt ($Na_2{}^{13}CO_3$) decomposed during the first charging process. The fragment at $m/z=45$ ($^{13}CO_2$) was not detected at any point in the charge-discharge process when $Na_2{}^{12}CO_3$ was added (**Figure S6**), thereby confirming that the observed $^{13}CO_2$ originated from the labeled $Na_2{}^{13}CO_3$. Simulta-

neously, $^{12}CO_2$ was detected during the evolution of $^{13}CO_2$, and the intensities of these two signals were comparable. It was therefore considered that despite replacing the carbon source of Na_2CO_3 with ^{13}C (purity of ^{13}C in $Na_2{}^{13}CO_3$ > 99%), $^{12}CO_2$ was also generated from the electrolyte, conductive carbon, binder, and separator components. Trace amounts of Na_2CO_3 could also have been present on the active material surface formed during the synthesis of P2–$Na_{2/3}Fe_{1/2}Mn_{1/2}O_2$, thereby further accounting for the observed generation of $^{12}CO_2$. However, $^{12}CO_2$ was not detected during the second charging cycle despite polarization to a high potential, suggesting that the generated $^{12}CO_2$ does not originate from simple oxidation of the electrolyte, conductive carbon, and/or other cell components. This $^{12}CO_2$ was therefore considered to have evolved through an electrolytic reaction that was induced by the addition of Na_2CO_3, as discussed later. In addition, the CV results presented in Figure 3 illustrate a noticeable increase in the irreversible oxidation current due to decomposition at voltages > 4.0 V. In the OEMS measurements, the intensity of CO_2 began to increase during the initial charge when the voltage of the full cell was 3.5 V. The corresponding potential of the positive electrode at this point was estimated to be ~4.0 V vs. Na^+/Na, as shown in **Figure S7**. This consistency further indicates that CO_2 gas was generated by the decomposition of Na_2CO_3.

To quantify the generation of CO_2 and O_2, the amount of gas produced during the charging and discharging processes in **Figure S6** was obtained by subtracting the background from the MS chromatogram and integrating it against the results obtained beyond ~3.5 V during the initial charging process until the end of the first discharge. In the initial cycle, 7.8 and 0.12 μmol of CO_2 and O_2 were generated, respectively, while in the second cycle, 0.28 and 0.029 μmol were generated, respectively. This could be accounted for by considering that the anodic decomposition of Na_2CO_3 proceeds via a two-electron reaction, analogous to a Li_2CO_3 decomposition reaction:[23]

$$Na_2CO_3 \rightarrow 2Na^+ + 2e^- + CO_2 + 1/2O_2 \quad (1)$$

Given that 4.0 μmol (~0.4 mg) of Na_2CO_3 was introduced into the positive electrode for the purpose of this experiment, the observed amount of CO_2 generated in the first cycle (7.8 μmol) was almost twice that of the theoretical amount calculated based on **Equation 1**, while the amount of O_2 generated was ~6.7% of the theoretical value. It was therefore considered unlikely that Na_2CO_3 decomposes via the two-electron reaction outlined in **Equation 1**. Moreover, the amount of CO_2 observed in the second cycle was only 3.6% of that observed in the first cycle, and it was expected that this CO_2 originated from solvent decomposition at high potentials. However, considering the decomposition of the solvent, the quantity of CO_2 produced in the initial cycle still exceeds that expected from the simple two-electron reaction presented in **Equation 1**, thereby suggesting that a side reaction involving the electrolyte contributes to the Na_2CO_3 decomposition process.

It was also found that operating the battery cell at a high potential led to the oxidation and decomposition of the EC and/or PC in the electrolyte. However, the extent of such oxidative decomposition at high potentials may be considered relatively small, given that a negligible amount of CO_2 was evolved in the second cycle. Other possible reactions have also been reported, including the reaction of oxygen radicals with EC.[30] Thus, based on the findings of this study, a mechanism for the oxidative decomposition of Na_2CO_3 as a sacrificial salt during the initial charging process is proposed, as shown in Figure 8. More specifically, the generated $NaCO_3^{\bullet}$ radical reacts with EC to produce two molecules of CO_2. The carbon atom of one of these CO_2 molecules is derived from Na_2CO_3, whereas the other is derived from the EC. Notably, the proposed route does not lead to the generation of O_2 gas. Importantly, the approximately overlapping gas evolution rates of $^{12}CO_2$ (*m/z* 44) and $^{13}CO_2$ (*m/z* 45) shown in Figure 7 are consistent with the proposed mechanism, while the negligible generation of O_2 further confirms that the reaction presented in **Equation 1** does not take place.

It should also be considered that Na_2CO_3 can react with the electrolyte. For example, the $NaPF_6$ component of the electrolyte can partially decompose according to the following reaction: $NaPF_6 \rightarrow NaF + PF_5$. Subsequently, the generated PF_5 can react with Na_2CO_3 ($PF_5 + Na_2CO_3 \rightarrow 2NaF + CO_2 + OPF_3$) to produce CO_2 and NaF. Indeed, such reactions between carbonates and PF_6-based electrolytes have also been reported in Li-ion batteries.[31] Thus, for the full cell system (see **Figure S8**), the HAXPES profile of the positive electrode and the SOXPES profile of the negative electrode recorded after the initial cycle indicate that decomposition products, such as NaF and $Na_xPF_yO_z$, are deposited on the electrode surface. Such decomposition

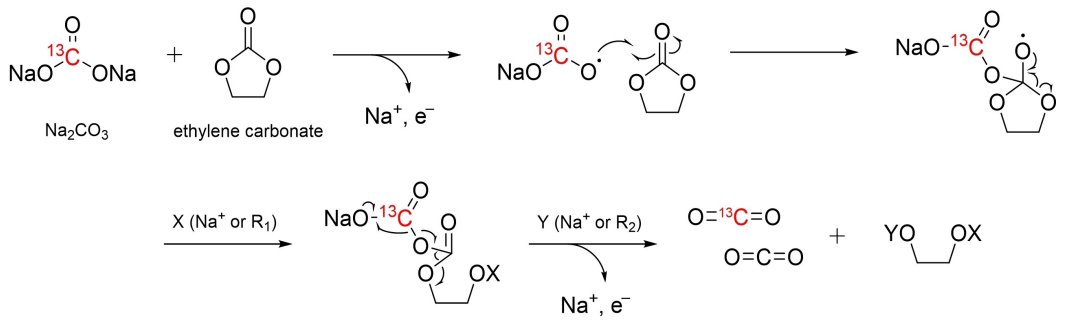

Figure 8. Decomposition mechanism of the Na_2CO_3 sacrificial salt in the full cell. R_1 and R_2 represent other carbonate species or their decomposition products.

Research Article
doi.org/10.1002/batt.202400009
Chemistry Europe
European Chemical Societies Publishing

products may also react with the electrolyte, thereby accounting for the slightly increased polarization observed in the cell containing added Na_2CO_3 (Figures 5, 6 and **S5**), along with the slightly decreased utilization of Na_2CO_3 (i.e., 88%, see Figure 5).

Finally, the full cell was disassembled after the initial discharge and the positive electrode was removed for measurement by XRD. The corresponding presented in Figure 9 confirm that the Na^+ generated from the decomposition of Na_2CO_3 during the initial charge was subsequently inserted into the positive electrode during the discharge process. More specifically, in the positive electrode with Na_2CO_3 addition (10 wt.%) the *00 l* peak is shifted to a higher 2θ value, whereas the *10 l* peak is shifted to a lower 2θ (cf., the system without Na_2CO_3 addition). These observations indicate that the *a*-axis of the unit lattice of P2-type $Na_{2/3}Fe_{1/2}Mn_{1/2}O_2$ is elongated, whereas the *c*-axis is shortened, owing to the suppressed repulsion between the transition metal oxide layers caused by the insertion of Na_2CO_3-derived Na^+ ions.

These results clearly demonstrate that Na^+ is supplemented into the cell following the electrochemical oxidative decomposition of the Na_2CO_3 sacrificial salt during the initial charge, which results in a high full-cell capacity even when utilizing a Na metal-free carbon material as the negative electrode. Although the average operating voltage of the full cell decreased from 2.85 to 2.58 V with the addition of Na_2CO_3 (possibly because of increased polarization), it is believed that further optimization of the Na_2CO_3-added electrode preparation could avoid such polarization. Moreover, the relatively large reversible capacity obtained following the addition of this sacrificial salt was found to successfully increase the energy density of the system from 270 to 315 Wh $kg_{(P2\text{–}FeMn)}^{-1}$, indicating its high overall performance and potential for application in sodium-ion batteries. Gas generated from sacrificial salts can be effectively released during the degassing process that follows the formation cycles in an industrial setting. In addition, this sacrificial salt can be applied in Na-ion capacitors based on activated carbon//HC cells.

3. Conclusions

Na_2CO_3 was introduced as a sacrificial salt into the Na-deficient layered oxide P2-type $Na_{2/3}Fe_{1/2}Mn_{1/2}O_2$ for use as a positive electrode material. It was found that the added Na_2CO_3 was electrochemically oxidized and decomposed at potentials >3.5 V vs. Na^+/Na. In addition, the full cell based on the Na_2CO_3-added P2-type $Na_{2/3}Fe_{1/2}Mn_{1/2}O_2$ as the positive electrode and hard carbon as the negative electrode exhibited a high capacity and an excellent capacity retention, indicating the successful decomposition of Na_2CO_3 and Na^+ supplementation in the full cell. Online electrochemical mass spectrometry (OEMS) measurements using ^{13}C-labeled $Na_2{}^{13}CO_3$ revealed that Na_2CO_3 decomposed during the initial charging process upon reaction with the ethylene carbonate in the electrolyte. As a result, CO_2 was generated from both the labelled $Na_2{}^{13}CO_3$ component ($^{13}CO_2$, $m/z=45$) and the ethylene carbonate ($^{12}CO_2$, $m/z=44$) in a 1:1 ratio ($^{12}CO_2$:$^{13}CO_2$). Although the direct oxidation of Na_2CO_3 typically forms both CO_2 and O_2, a peak at $m/z=32$ (O_2) was not observed by OEMS, which suggests the absence of a direct oxidation reaction. Overall, this study demonstrates the effectiveness of using Na_2CO_3 as a sacrificial salt to increase the capacities of sodium-ion batteries, and its incorporation is beneficial from the perspectives of both safety and cost.

Experimental

Electrode preparation

1 g of Na_2CO_3 was initially dry-mixed and crushed via ball milling at 1300 rpm for 1 h using 14 g of ZrO_2 balls (φ1.0 mm) prior to drying at 200 °C under vacuum. The P2-type $Na_{2/3}Fe_{1/2}Mn_{1/2}O_2$ material was synthesized via a solid-state reaction.[5] For this purpose, stoichiometric ratios of Fe_2O_3 (99.9%, FUJIFILM Wako Pure Chemical Corporation) and Mn_2O_3 prepared by calcining $MnCO_3$ (44% Mn content, Kishida Chemical Co., Ltd.) at 700 °C in air, were mixed with a 5 mol% excess of Na_2CO_3 (99.8%, Nacalai Tesque, Inc.) via ball milling in acetone at 600 rpm for 12 h. After this time, the mixture was dried to give a powder, which was subsequently pelletized, subjected to calcination at 900 °C for 12 h, and then quenched by quickly transferring the pellet from the heated

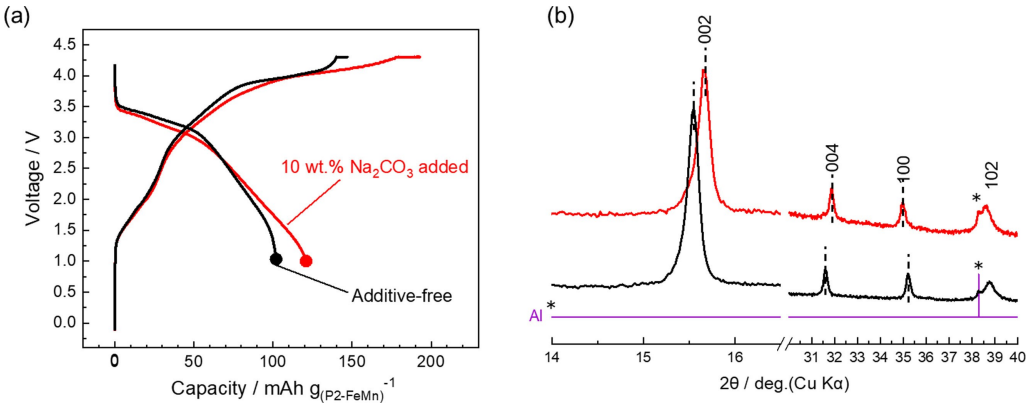

Figure 9. (a) Charge-discharge curves recorded for the HC//P2–$Na_{2/3}Fe_{1/2}Mn_{1/2}O_2$ full cells with and without 10 wt.% Na_2CO_3 addition. (b) XRD patterns of the P2–$Na_{2/3}Fe_{1/2}Mn_{1/2}O_2$ electrode with and without 10 wt.% Na_2CO_3 addition, as obtained from each full cell after the initial cycle.

furnace to an Ar-filled glove box. Following analysis by X-ray diffraction (see **Figure S9**), it was apparent that all diffraction lines could be attributed to the $P6_3/mmc$ space group, thereby confirming the formation of single-phase P2-type $Na_{2/3}Fe_{1/2}Mn_{1/2}O_2$. In addition, Co_3O_4, which was used as the electrocatalyst,[28] was synthesized by calcining $Co(OH)_2$ (Kishida Chemical Co., Ltd.) at 700 °C for 12 h under air.

The positive electrode consisted of a mixture of active material, Na_2CO_3, acetylene black (AB, Denka Li-400), and polyvinylidene fluoride (PVDF, Solvay Japan, Ltd.) in a ratio of (80-*x*):*x*:10:10 (wt.%), where $x = 0$, 5, and 10 wt.%. By adding an adequate amount of *N*-methyl pyrrolidone (NMP) into the mixed powder, a slurry was obtained. This slurry was coated onto an Al foil and dried at 80 °C in vacuum. The electrode sheet was punched into a disk to form the composite electrode. The diameter of the disk was 10 mm in the R2032 coin cell and 15 mm in the three-electrode cell (SB9, EC FRONTIER). The working electrode was incorporated into the coin cell and the three-electrode cell using a glass fiber separator (BG-100R, ADVANTEC, Co.) that was soaked with a 1.0 mol dm^{-3} $NaPF_6$ solution prepared in a mixture of ethylene carbonate and propylene carbonate (EC/PC, 1:1, v/v, Kishida Chemical Co.). Na metal (>99%, Kanto Chemical Co., Ltd.) was used as the counter/reference electrode in the half-cell. In the full cell, a hard-carbon electrode was used as the negative electrode. More specifically, the negative electrode consisted of a mixture of Carbotron P(J) (KUREHA Co.), acetylene black (Denka Li-400), and sodium polyacrylate (Kishida Chemical Co., Ltd.) in a ratio of 85:10:5 (wt.%) and mixed with an adequate amount of deionized water. The slurry was coated onto an Al foil and dried at 80 °C for 2 h under air and then at 150 °C overnight under vacuum. The active material loading for the full cell ranged from 1.5 to 2.6 mg cm^{-2} for P2–NiMn and from 1.0 to 1.3 mg cm^{-2} for the hard carbon. Electrochemical tests were performed in a thermostatic chamber at 25 °C. The voltage ranges for charge-discharge tests were 1.5–4.3 V vs. Na^+/Na (in a half cell with a positive electrode), 0.002–2.0 V vs. Na^+/Na (in a half cell with a negative electrode), or 1.0–4.3 V (in a full cell, adjusted the lower cut-off voltage downwards to enhance the reversible capacity) at a current density of 0.02 mA cm^{-2}. For certain cells, a constant current introduced in the constant voltage (CC–CV) mode was employed for the initial charging process, as described below. Cyclic voltammetry (CV) was also performed at 0.3 mV s^{-1} and 25 °C.

Characterization

The structure of the as-synthesized P2-type $Na_{2/3}Fe_{1/2}Mn_{1/2}O_2$ was estimated from powder XRD measurements (SmartLab, Rigaku Co.) using Cu Kα irradiation (45 mA, 40 kV). A purpose-built airtight sample holder was used for the XRD measurements to prevent exposure to air. The particle morphology was observed using scanning electron microscopy (SEM-EDS, JCM-6000, JEOL Ltd.) at an acceleration voltage of 15 kV. The surface species present on the fresh and cycled electrodes were investigated by soft X-ray photoelectron spectroscopy (SOXPES) and hard X-ray photoelectron spectroscopy (HAXPES). SOXPES was conducted using a VersaProbe II (ULVAC-PHI) instrument equipped with an Al X-ray source (1486.6 eV), while HAXPES was conducted at a high excitation energy (7938.9 eV) using a VG-SCIENTA photoelectron energy analyzer (R-4000) at the BL46XU facility in SPring-8, Japan.[32] The binding energy of the obtained spectrum was calibrated and normalized to that of the sp^2 carbon peak in graphite (284.5 eV).

Using online electrochemical mass spectrometry (OEMS), the gaseous and volatile species released from the battery cell through the anodic decomposition of Na_2CO_3 were detected during the electrochemical measurements.[33] Additionally, $Na_2{}^{13}CO_3$ (chemical purity >98%, ^{13}C purity >99%, Cambridge Isotope Laboratories, Inc.) was also employed for MS measurements. The test cell (gas-flow cell for OEMS, custom-ordered at the EC Frontier) was assembled in a glovebox under an Ar atmosphere and connected to a gas chromatograph-mass spectrometer (GCMS-QP2020 NX, Shimadzu) in a columnless configuration to enable simultaneous electrochemical and MS measurements (quadrupole detector). He (99.99995%) was used as the carrier gas. For all OEMS intensity data, the signal was normalized to the measured intensity at $m/z = 219$ (standard sample of perfluorotributylamine) prior to each experiment to facilitate a numerical comparison of the signal intensities recorded for the different experiments. In addition, for the $m/z = 32$ and 44 signals (assigned to O_2 and $^{12}CO_2$, respectively), the system was calibrated to allow complete quantitative measurements. All calibrations were conducted using standard gases, and mixed gases were allowed to flow into the MS system through separate lines. The O_2 and $^{12}CO_2$ concentrations were controlled by varying the ratio of the mixed gas to pure He, and the MS intensities at all concentrations were recorded. The calibration curves were generated accordingly. Quantitative calculations for m/z 45 ($^{13}CO_2$) were conducted assuming that the sensitivity toward m/z 45 ($^{13}CO_2$) was identical to that toward m/z 44 ($^{12}CO_2$). The validity of the above assumption was confirmed using the calibration curves for $m/z = 44$ and 45 obtained using the CO_2/He mixed standard gas; the calibration slope for $m/z = 45$ was 1.2% of the sum of those obtained for $m/z = 44$ and 45, which is in agreement with the natural abundance of ^{13}C (1.1%) (**Figure S10**).[34] In addition, background subtraction and data smoothing were conducted using a Savitzky-Golay filter for the selected ion chromatograms presented herein.

Acknowledgements

This study was partially supported by the JSPS KAKENHI (grant numbers 20H02849, 21K14724, 22K14772, and 23K13829). The synchrotron radiation experiments were performed at the BL46XU beamline of SPring-8 with the approval of the Japan Synchrotron Radiation Research Institute (JASRI) under proposal numbers 2019B1850 and 2021B1874. The SOXPES measurements were performed at the National Institute for Materials Science (NIMS) Battery Research Platform under JST Grant Number JPMJPF2016.

Conflict of Interests

The authors declare no competing financial interests.

Data Availability Statement

The data that support the findings of this study are available from the corresponding author upon reasonable request.

Keywords: Na-ion battery · Sacrificial additive · Layered oxide · Sodium carbonate

[1] a) N. Yabuuchi, K. Kubota, M. Dahbi, S. Komaba, *Chem. Rev.* **2014**, *114*, 11636–11682; b) K. Kubota, S. Komaba, *J. Electrochem. Soc.* **2015**, *162*, A2538–A2550; c) K. Kubota, M. Dahbi, T. Hosaka, S. Kumakura, S. Komaba, *Chem. Rec.* **2018**, *18*, 459–479; d) H. Zhao, J. Wang, Y. Zheng, J.

Li, X. Han, G. He, Y. Du, *Angew. Chem. Int. Ed.* **2017**, *56*, 15334–15338; e) J. Xia, H. Zhao, W. K. Pang, Z. Yin, B. Zhou, G. He, Z. Guo, Y. Du, *Chem. Sci.* **2018**, *9*, 3421–3425; f) Z. Liu, Y. Zhang, H. Zhao, N. Li, Y. Du, *Sci. China Mater.* **2016**, *60*, 167–177.
[2] a) C. Delmas, C. Fouassier, P. Hagenmuller, *Physica B+C* **1980**, *99*, 81–85; b) C. Delmas, J. Braconnier, C. Fouassier, P. Hagenmuller, *Solid State Ionics* **1981**, *3–4*, 165–169; c) K. Kubota, S. Kumakura, Y. Yoda, K. Kuroki, S. Komaba, *Adv. Energy Mater.* **2018**, *8*, 1703415.
[3] S. Komaba, T. Nakayama, A. Ogata, T. Shimizu, C. Takei, S. Takada, A. Hokura, I. Nakai, *ECS Trans.* **2009**, *16*, 43–55.
[4] K. Kubota, T. Asari, H. Yoshida, N. Yaabuuchi, H. Shiiba, M. Nakayama, S. Komaba, *Adv. Funct. Mater.* **2016**, *26*, 6047–6059.
[5] N. Yabuuchi, M. Kajiyama, J. Iwatate, H. Nishikawa, S. Hitomi, R. Okuyama, R. Usui, Y. Yamada, S. Komaba, *Nat. Mater.* **2012**, *11*, 512–517.
[6] a) D. A. Stevens, J. R. Dahn, *J. Electrochem. Soc.* **2000**, *147*, 1271; b) S. Komaba, W. Murata, T. Ishikawa, N. Yabuuchi, T. Ozeki, T. Nakayama, A. Ogata, K. Gotoh, K. Fujiwara, *Adv. Funct. Mater.* **2011**, *21*, 3859–3867; c) M. Dahbi, N. Yabuuchi, K. Kubota, K. Tokiwa, S. Komaba, *Phys. Chem. Chem. Phys.* **2014**, *16*, 15007–15028.
[7] S. Komaba, T. Ishikawa, N. Yabuuchi, W. Murata, A. Ito, Y. Ohsawa, *ACS Appl. Mater. Interfaces* **2011**, *3*, 4165–4168.
[8] E. Peled, *J. Electrochem. Soc.* **1979**, *126*, 2047–2051.
[9] D. Dewar, A. M. Glushenkov, *Energy Environ. Sci.* **2021**, *14*, 1380–1401.
[10] H. Park, M. Kim, F. Xu, C. Jung, S. M. Hong, C. M. Koo, *J. Power Sources* **2015**, *283*, 68–73.
[11] X. Sun, X. Zhang, H. Zhang, N. Xu, K. Wang, Y. Ma, *J. Power Sources* **2014**, *270*, 318–325.
[12] H. Wang, Y. Xiao, C. Sun, C. Lai, X. Ai, *RSC Adv.* **2015**, *5*, 106519–106522.
[13] I. Moeez, H.-G. Jung, H.-D. Lim, K. Y. Chung, *ACS Appl. Mater. Interfaces* **2019**, *11*, 41394–41401.
[14] a) G. Singh, B. Acebedo, M. C. Cabanas, D. Shanmukaraj, M. Armand, T. Rojo, *Electrochem. Commun.* **2013**, *37*, 61–63; b) J. Martinez De Ilarduya, L. Otaegui, J. M. López del Amo, M. Armand, G. Singh, *J. Power Sources* **2017**, *337*, 197–203.
[15] B. Zhang, R. Dugas, G. Rousse, P. Rozier, A. M. Abakumov, J.-M. Tarascon, *Nat. Commun.* **2016**, *7*, 10308.
[16] X. Pan, A. Chojnacka, P. Jeżowski, F. Béguin, *Electrochim. Acta* **2019**, *318*, 471–478.
[17] a) D. Shanmukaraj, K. Kretschmer, T. Sahu, W. Bao, T. Rojo, G. Wang, M. Armand, *ChemSusChem* **2018**, *11*, 3286–3291; b) M. Arnaiz, D. Shanmukaraj, D. Carriazo, D. Bhattacharjya, A. Villaverde, M. Armand, J. Ajuria, *Energy Environ. Sci.* **2020**, *13*, 2441–2449.
[18] K. Zou, P. Cai, Y. Tian, J. Li, C. Liu, G. Zou, H. Hou, X. Ji, *Small Methods* **2020**, *4*, 1900763.
[19] Y. B. Niu, Y. J. Guo, Y. X. Yin, S. Y. Zhang, T. Wang, P. Wang, S. Xin, Y. G. Guo, *Adv. Mater.* **2020**, *32*, 2001419.
[20] C.-H. Jo, J. U. Choi, H. Yashiro, S.-T. Myung, *J. Mater. Chem. A* **2019**, *7*, 3903–3909.
[21] M. Sathiya, J. Thomas, D. Batuk, V. Pimenta, R. Gopalan, J.-M. Tarascon, *Chem. Mater.* **2017**, *29*, 5948–5956.
[22] Y. Qiao, H. Yang, Z. Chang, H. Deng, X. Li, H. Zhou, *Nat. Energy* **2021**, *6*, 653–662.
[23] C. Tan, A. Wang, D. Cao, F. Yu, Y. Wu, X. He, Y. Chen, *Adv. Energy Mater.* **2023**, *13*, 2204191.
[24] C. Sun, X. Zhang, C. Li, K. Wang, X. Sun, Y. Ma, *J. Power Sources* **2021**, *515*, 10.1016/j.jpowsour.2.
[25] J. A. Cella, S. W. Bacon, *J. Org. Chem.* **1984**, *49*, 1122–1125.
[26] L. A. Ma, A. J. Naylor, L. Nyholm, R. Younesi, *Angew. Chem. Int. Ed.* **2021**, *60*, 4855–4863.
[27] M.-l. Qin, C.-y. Yin, W. Xu, Y. Liu, J.-h. Wen, B. Shen, W.-g. Wang, W.-m. Liu, *Trans. Nonferrous Met. Soc. China* **2021**, *31*, 2074–2080.
[28] N. Yabuuchi, K. Yoshii, S.-T. Myung, I. Nakai, S. Komaba, *J. Am. Chem. Soc.* **2011**, *133*, 4404–4419.
[29] N. Yoshinaga, S. Kumakura, K. Kubota, T. Horiba, S. Komaba, *J. Electrochem. Soc.* **2019**, *166*, A5430–A5436.
[30] a) J. Zhao, X. Zhang, Y. Liang, Z. Han, S. Liu, W. Chu, H. Yu, *ACS Energy Lett.* **2021**, *6*, 2552–2564; b) I. A. Shkrob, Y. Zhu, T. W. Marin, D. Abraham, *J. Phys. Chem. C* **2013**, *117*, 19255–19269.
[31] B. Wu, Y. Ren, D. Mu, X. Liu, F. Wu, *J. Power Sources* **2014**, *272*, 183–189.
[32] a) N. Yabuuchi, K. Shimomura, Y. Shimbe, T. Ozeki, J.-Y. Son, H. Oji, Y. Katayama, T. Miura, S. Komaba, *Adv. Energy Mater.* **2011**, *1*, 759–765; b) R. Tatara, T. Umezawa, K. Kubota, T. Horiba, R. Takaishi, K. Hida, T. Matsuyama, S. Yasuno, S. Komaba, *ChemElectroChem* **2021**, *8*, 4345–4352.
[33] a) H. M. Kwon, M. L. Thomas, R. Tatara, Y. Oda, Y. Kobayashi, A. Nakanishi, K. Ueno, K. Dokko, M. Watanabe, *ACS Appl. Mater. Interfaces* **2017**, *9*, 6014–6021; b) Y. Ugata, R. Tatara, T. Mandai, K. Ueno, M. Watanabe, K. Dokko, *ACS Appl. Energy Mater.* **2021**, *4*, 1851–1859, 10.1021/acsaem.0c029.
[34] M. Metzger, C. Marino, J. Sicklinger, D. Haering, H. A. Gasteiger, *J. Electrochem. Soc.* **2015**, *162*, A1123–A1134.

Manuscript received: January 9, 2024
Revised manuscript received: February 5, 2024
Accepted manuscript online: February 9, 2024
Version of record online: March 12, 2024